

# An estimation of static aerodynamic forces of box girders using computational fluid dynamics

Shigeru Watanabe<sup>†</sup>

*Research & Development Headquarters, Mitsui Engineering & Shipbuilding Co., Ltd., Okayama, Japan*

Hiroo Inoue<sup>‡</sup>

*Structure & Logistic Systems Headquarters, Mitsui Engineering & Shipbuilding Co., Ltd., Tokyo, Japan*

Koichiro Fumoto<sup>‡†</sup>

*Public Works Research Institute Independent Administrative Institution, Ibaraki, Japan*

*(Received July 30, 2003, Accepted January 5, 2004)*

**Abstract.** This study has focused on aerodynamics for a wind-resistance design about the single and tandem box girder sections to realize a super-long span bridge in the near future. Three-dimensional static analysis of flows around the fundamental single and tandem box girder sections with fairing is carried out by means of the IBTD/FS finite element technique with LES turbulence model. As the results of the analysis, computations have verified aerodynamic characteristics of both sections by the histories of aerodynamic forces, the separation and reattachment flow patterns and the surface pressure distributions. The relationship between the section shapes and the aerodynamic characteristics is also investigated in both sections. And the mechanism about the generation of fluctuating aerodynamic forces is discussed.

**Keywords:** CFD; LES; FEM; box girder section; fairing; aerodynamics.

---

## 1. Introduction

In recent years, aerodynamics for a wind-resistance design about many types of the box girder bridge sections (Diana, *et al.* 1999, Hui and Larsen 2002) have been examined by wind tunnel tests so as to realize a super-long span bridge in the near future. When compared with aerodynamic characteristics between single and tandem box girders, the fact that tandem girders have a tendency to excel single girders in a wind-resistance stability has been gradually understood after a long series of experiments (Ogawa, *et al.* 2002, Sato, *et al.* 2002). Since a main aim of a wind tunnel test is an estimation of flutter speed, however, few papers (Matsumoto, *et al.* 1999) have published on related the mechanism about the generation of the aerodynamic forces and the improvement of the wind-resistance stability.

---

<sup>†</sup> Research Engineer

<sup>‡</sup> General Manager

<sup>‡†</sup> Senior Researcher

On the other hand, in the course of progress of computer, a computational analysis is tried to introduce in various branches of engineering. And along with developments of analytical techniques, Computational Fluid Dynamics (CFD) is widely applied to establish aerodynamics for a wind-resistance design. If an examination method by CFD is established and CFD is available for a pilot research of a wind tunnel test, it will be possible not only to reduce costs of experiments but also to enhance understanding of aerodynamic characteristics. In the progress of CFD, flows around circular and rectangular cylinders have been calculated in two and three-dimensional space (Tamura, *et al.* 1995, Hirano, *et al.* 1999) and the results have been compared to the experimental data obtained by the wind tunnel (Nakaguchi, *et al.* 1968, Bearman and Trueman 1972) through many years. Hirano *et al.* and these writers point out that, large fluctuations are observed in the two-dimensional analysis, and this is one of the factors in the overestimation or underestimation of aerodynamic forces in two-dimensional analysis (Hirano, *et al.* 1999). Carrying out three-dimensional analysis was too heavy burden on a general-purpose computer, however, the flow around the bridge sections has been calculated by two-dimensional analysis adopted Reynolds Averaged Navier-Stokes (RANS) turbulence model (Shirai and Ueda 2001, Xiang and Ge 2002). Recently a general-purpose computer in itself has made remarkable progress in the computational efficiency and a cluster computing through a network system has been easily done little by little. Thus a small scale three-dimensional analysis has come into common use in a wind-resistance design.

Taking the above background into account, as a new approach of our researches, this paper reports on three-dimensional numerical simulations of the flow around the fundamental box girder sections. The analysis of unsteady flows around the box girder sections are carried out in the three-dimensional space. As for the basic equations of the incompressible viscous flow around the box girder sections, the incompressible Navier-Stokes equations are employed. The momentum and continuity equations are discretized by the IBTD/FS(Improved Balancing Tensor Diffusivity (Maruoka, *et al.* 1999) / Fractional Step (Hayashi, *et al.* 1991)) finite element technique. And the large eddy simulation (LES) with the Smagorinsky sub-grid scale (SGS) model is applied for the turbulence model.

As the results of the analysis, we have succeeded in precisely simulating flow patterns, such as behaviors of the vortex motions around the single and tandem box girder sections. The analysis has verified aerodynamic characteristics by the histories of aerodynamic forces, the separation and reattachment flow patterns and the surface pressure distributions. The relationship between the section shapes and aerodynamic characteristics is also investigated in cases of the single and tandem box girder sections. And the mechanism about the generation of fluctuating aerodynamic forces is discussed. The generating mechanism of fluctuating aerodynamic forces on the single and tandem box girder sections is quite different from each other. We find out, in case of the single box girder section, Karman vortex separated from the trailing edge makes a contribution to the aerodynamic characteristic. On the other hand, the flows in the central open space influence on the aerodynamic characteristic of the tandem girder section.

## 2. Basic equations

### 2.1. Governing equations

Let  $\Omega$  denote the spatial domain and  $\Gamma$  denote the boundary of  $\Omega$ . The incompressible Navier-Stokes equations governing incompressible viscous flow can be written as the non-dimensional form

of momentum and continuity equations,

$$\rho \left( \frac{\partial \mathbf{u}}{\partial t} + \mathbf{u} \cdot \nabla \mathbf{u} - \mathbf{f} \right) - \nabla \cdot \boldsymbol{\sigma}(p, \mathbf{u}) = \mathbf{0} \text{ on } \Omega \quad (1)$$

$$\nabla \cdot \mathbf{u} = 0 \text{ on } \Omega \quad (2)$$

where  $\rho$  is density,  $\mathbf{u}$  and  $p$  are velocity and pressure,  $\boldsymbol{\sigma}$  is stress tensor that is specified as:

$$\boldsymbol{\sigma}(p, \mathbf{u}) = -p\mathbf{I} + 2\mu\boldsymbol{\varepsilon}(\mathbf{u}), \quad \boldsymbol{\varepsilon}(\mathbf{u}) = \frac{1}{2}(\nabla \mathbf{u} + (\nabla \mathbf{u})^T) \quad (3)$$

where  $\mathbf{I}$  and  $\mu$  are the identity tensor and the coefficient of viscosity.

Dirichlet and Neumann boundary conditions are specified as:

$$\mathbf{u} = \mathbf{g} \text{ on } \Gamma_g \quad (4)$$

$$\mathbf{n} \cdot \boldsymbol{\sigma} = \mathbf{h} \text{ on } \Gamma_h \quad (5)$$

where  $\mathbf{n}$  is the unit outward normal vector to  $\Gamma$ .

## 2.2. Smagorinsky SGS model

In case of introducing of the Smagorinsky SGS (Sub-Grid Scale) model, the basic equations are substituted for the incompressible Navier-Stokes equations filtered with a conception of LES (Large Eddy Simulation).

Then the value of each variable is the grid mean. And kinematic eddy viscosity of SGS component, that is specified as follows, is added to the viscous term.

$$\nu_t = (C_s h)^2 (2\varepsilon_{ij}^2)^{\frac{1}{2}} \quad (6)$$

where  $C_s$  is a Smagorinsky constant,  $h$  is the range of filter. And  $h$  multiplied by the wall dumping function of Van Driest ( $1 - \exp(-y^+/25)$ ) in the close to the wall surface.

## 2.3. Temporal and spatial discretizations

The IBTD/FS finite element formulation is introduced for the methodology of the numerical flow simulation. The Crank-Nicholson method is applied to momentum Eq. (1) and the continuity Eq. (2) is treated as the full implicit scheme for the temporal discretization. The improved balancing tensor diffusivity (IBTD) method (Maruoka, *et al.* 1999) is employed for the spatial discretization of the momentum Eq. (1). The fractional step (FS) method (Hayashi, *et al.* 1991) is applied to satisfying the continuity Eq. (2). In the FS method, the velocity and pressure are separately calculated by the momentum equation. In case of the IBTD method, the artificial diffusion term consists of the advection term and pressure gradient term.

As the result of this, the second-order accuracy is secured in both the temporal and spatial direction, and the numerical dissipation and phase error can be reduced. Since the finite element

equations is symmetric, the computational efficiency is very high and this method is quite effective to three-dimensional computations.

### 3. Analytical condition

In this paper, the numerical fluid flow analysis around the fundamental single and tandem box girder sections with fairing is carried out for discussing aerodynamic characteristics for the wind-resistance design.

Fig. 1 and Table 1 show the models of both the single and tandem box girder sections and analytical conditions, respectively. The width  $B$  and the height  $D$  of box girder sections are taken as representative length. The single section shown in Fig. 1(a) is combined with a rectangular cylinder with a side ratio ( $B/D$ ) of 15.1 and two equilateral triangles. The length of the base of the triangle is the same as the height of girder ( $1.0D$ ). And the tandem section shown in Fig. 1(b) has the central open space of  $3.8D$ . Fig. 2 and Fig. 3 show the analytical domain and the enlarged finite element meshes close to girder sections, respectively. The attack angle  $\alpha$  to  $x$  axis is set 0 degree. The

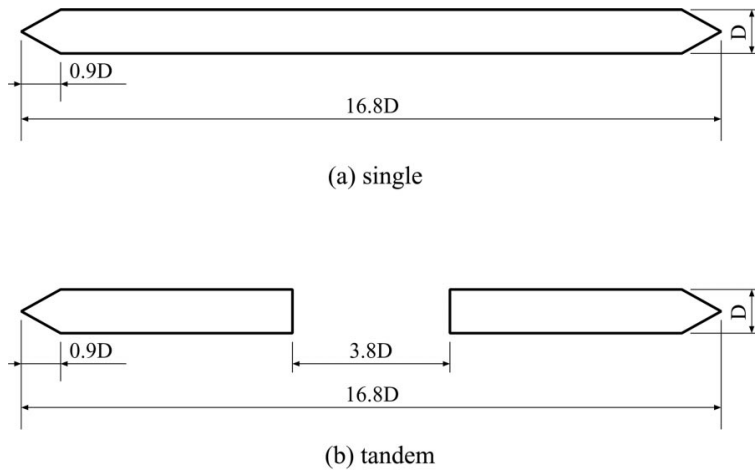


Fig. 1 Section models

Table 1 Analytical conditions

Side ratio	$B/D=16.8$
Reynolds number	$Re=1.0\times 10^4$
Time increment	$\Delta t=0.05D/U$
Smagorinsky constant	$C_s=0.13$
Division length of span axis	$\Delta_x=0.1D$
Division number of span axis	64
Total number of elements	single : 1,982,464 tandem : 2,069,504
Total number of nodes	single : 2,042,560 tandem : 2,132,195
Minimum element length	$5.78\times 10^{-3}D$

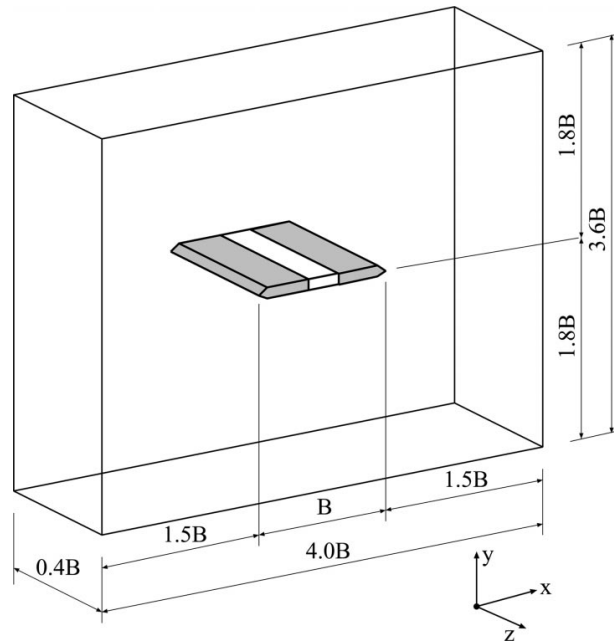


Fig. 2 Analytical domain

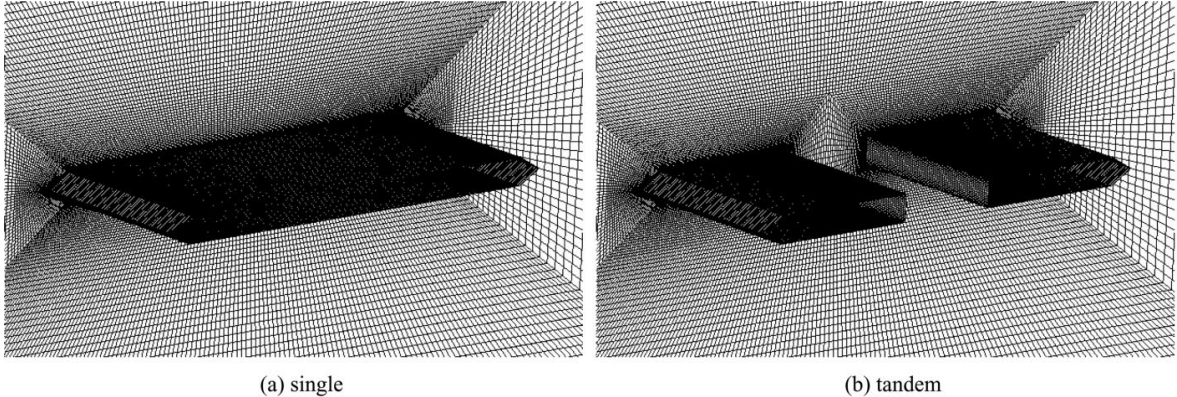


Fig. 3 Finite element mesh (enlarged)

section length of  $z$  direction is set  $0.4B$ . The area is divided into 64 equal parts with the layer dividing width in the axis direction  $z$  at  $0.1D$ .

As to the boundary conditions, Dirichlet boundary of inflow  $U$  is set at the left end on  $y$ - $z$  plane, non-slip condition around the box girder section, and slip condition at the upper and lower boundary on  $x$ - $y$  plane. In addition, the periodic boundary condition is specified on the ends of  $x$ - $y$  plane. In order to let vortex flow through the end of boundary smoothly, the boundary condition of advection type is introduced at the right end.

## 4. Results and discussions

### 4.1. History of three components of fluid force coefficient

#### 4.1.1. Comparison with single and tandem

At first, fluid forces acting on the box girder sections are represented by an ordinary three components of fluid force coefficients as:

$$Cd = \frac{F_d}{0.5\rho U^2 D} \quad (7)$$

$$Cl = \frac{F_l}{0.5\rho U^2 B} \quad (8)$$

$$Cm = \frac{F_m}{0.5\rho U^2 B^2} \quad (9)$$

where  $F_d$ ,  $F_l$  and  $F_m$  are drag force, lift force and pitching moment, respectively.

A coordinate axis of  $Cd$ ,  $Cl$  and  $Cm$  is defined in Fig. 4, upward of  $Cl$  and clockwise of  $Cm$  are positive directions, respectively. Fig. 5 shows the histories of three components of fluid force coefficient comparing the single and tandem box girder sections. Fig. 5(a) and Fig. 5(b) are the results of single and tandem box girder sections, respectively.

As comparison of histories between the single and tandem sections, the mean value of  $Cd$  on the tandem box girder section is about twice as large as the single's one. The fluctuating amplitudes of  $Cl$  and  $Cm$  of the tandem section are about 10 times the single's one. And the phase difference of between  $Cl$  and  $Cm$  is inversion in regard to both the single and tandem sections. These phenomena will be discussed later by surface pressure distributions.

Fig. 6 shows the amplitude of Fourier spectrum vs. non-dimensional frequency of  $C_{fr}$ . The non-dimensional frequency of  $C_{fr}$  is defined as:

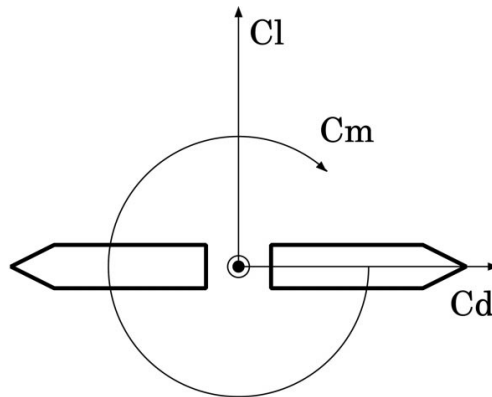


Fig. 4 Coordinate axis of three components of fluid force coefficient

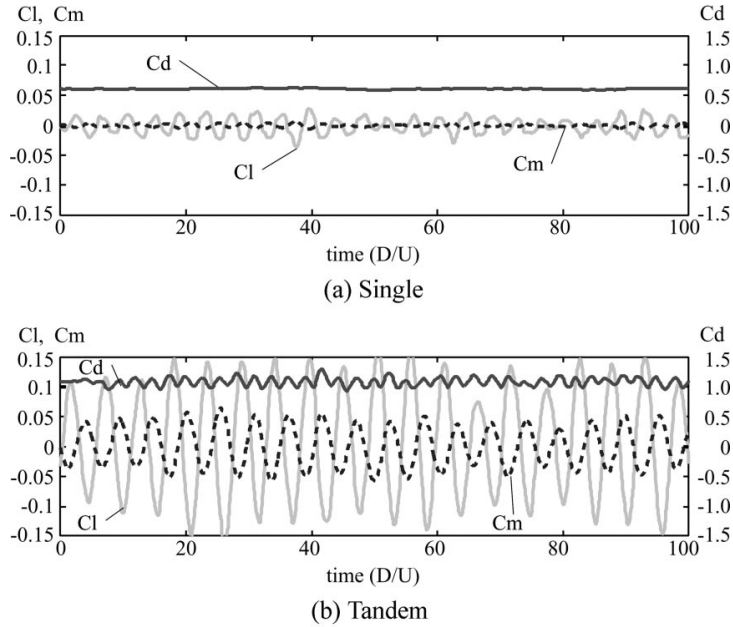


Fig. 5 Three components of fluid force coefficient

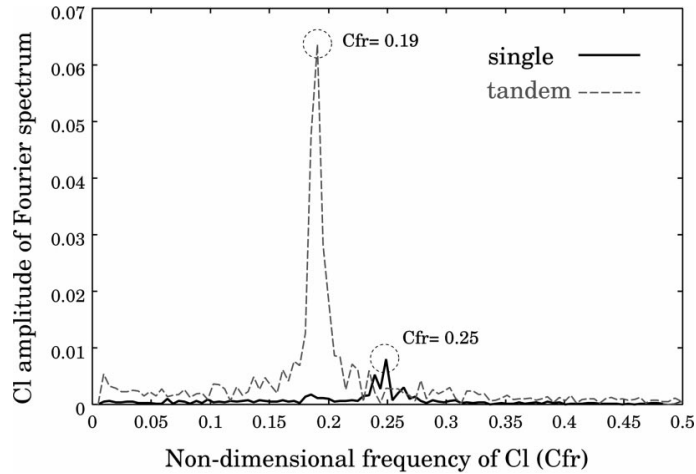


Fig. 6 Distribution of Fourier spectrum of  $C_l$

$$C_{fr} = \frac{F_{fr}D}{U} \quad (10)$$

where  $F_{fr}$  is the frequency of lift force.

$C_{fr}$  of the single and tandem sections are 0.25, 0.19, respectively. It shows that the single's frequency increases by 30% with the tandem's one. And the peak  $C_l$  amplitude of the tandem section at  $C_{fr} = 0.19$  is about 10 times as high as the single's one at 0.25. Then it can be considered that two histories of three components are quite different from each other.

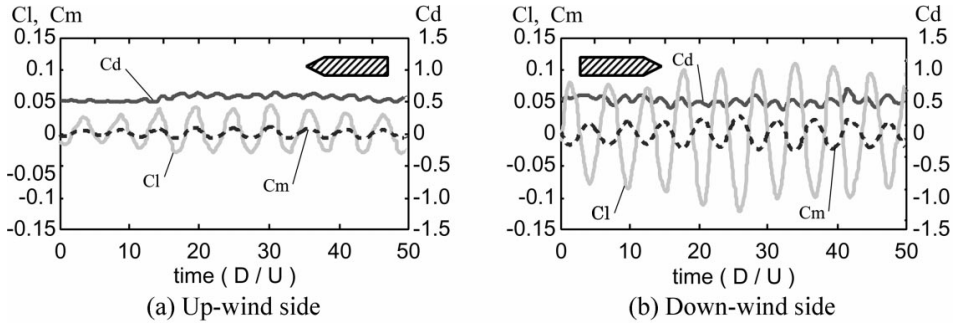


Fig. 7 Separation of three components of fluid force coefficient

#### 4.1.2. Separation of up and down wind side sections

As for the tandem section, the fluid forces acting on each up and down wind side section are investigated in detail. Fig. 7 shows each individual history of three components of fluid force coefficient. Fig. 7(a) and Fig. 7(b) are the histories of up and down wind side sections, respectively. The mean value of  $C_d$  on up and down wind side sections is almost equal between the two sides, then whole  $C_d$  is shared among two sides. On the other hand, the fluctuating amplitudes of  $C_l$  and  $C_m$  on the down-wind side section are about 4 times as large as the up-wind side amplitudes. As to the phase difference of between  $C_l$  and  $C_m$ , Fig. 7(a) up and (b) down wind side are in phase and out of phase, respectively. Since the phase difference of between whole  $C_l$  and  $C_m$  is inversion shown in Fig. 5(b), the fluid forces acting on down-wind side section controls the whole harmonic forces of  $C_l$  and  $C_m$ .

### 4.2. Instantaneous state of flow

#### 4.2.1. Instantaneous vorticity

Fig. 8 shows the bird's-eye view of instantaneous vorticities ( $\omega_z = \pm 2.0$ ). The flows separated from the front fairing reattach to the each upper and lower side around  $B/D=3$ , in common with Fig. 8(a),(b), and vorticities are occurred around reattachment points. In case of the single section, the only small eddying is occurred at the trailing edge after the separation-reattachment at leading edge. On the other hand, in case of the tandem section, the flows are separated from the trailing corners of up-wind side section and the large-scale separation-reattachment phenomena at the leading corners of the down-wind side section are confirmed.

#### 4.2.2. Particle trace

Fig. 9 shows the bird's-eye view of the particle trace from 3 points ( $x=-12.5$ ,  $y=+0.25$ ,  $z=+1.6$ ,  $+3.2$ ,  $+4.8$ ). In case of the single section, one particle is rotating at the trailing edge. But the stream around the single section is simple comparatively. On the other hand, in case of the tandem section, one particle is involved at the trailing corner of up-wind side section and the particle crosses over to the other side. Thus the flow in the central open space is very complex. It can be considered that

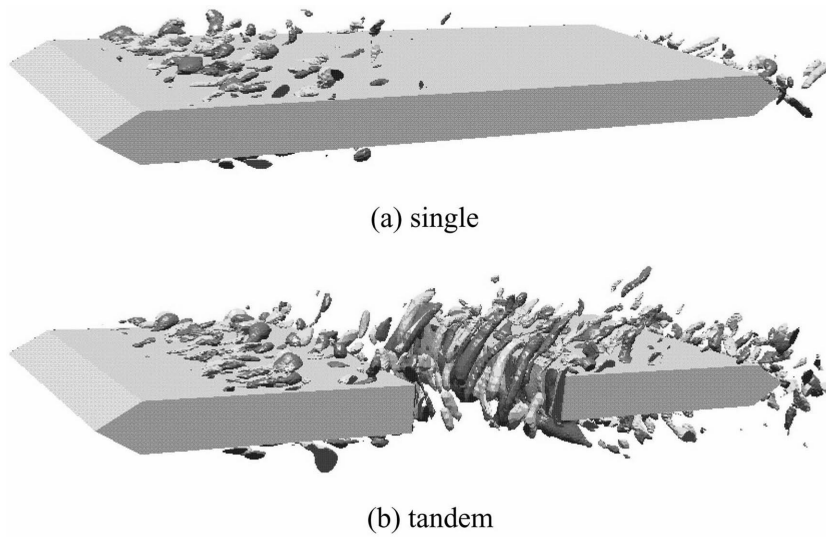


Fig. 8 Bird's-eye view of instantaneous vorticity ( $\omega_z = \pm 2.0$ )

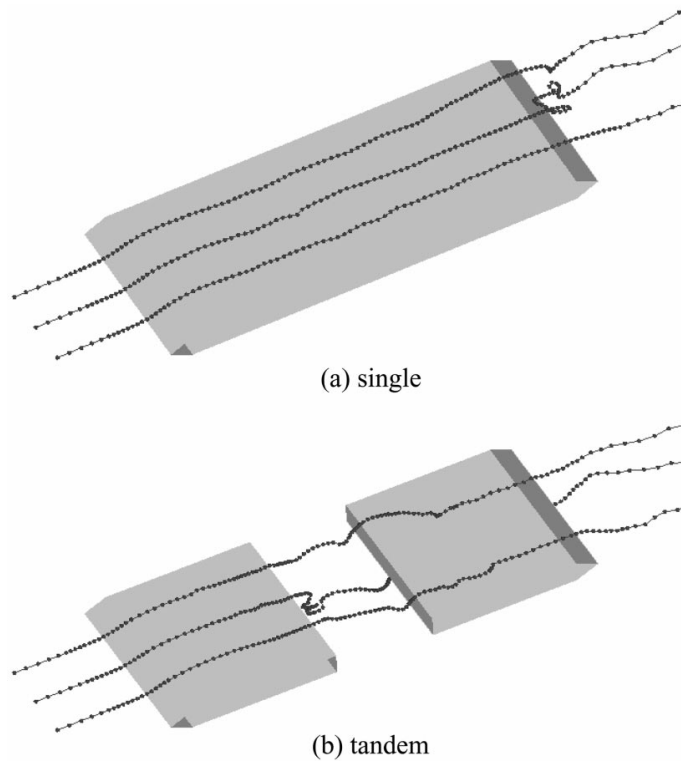


Fig. 9 Bird's-eye view of particle trace

the both flow patterns are also different from each other according to the presence of the central open space.

### 4.3. Surface pressure distribution

Fig. 10 shows the surface pressure distributions of the single and tandem sections. The non-dimensional pressure coefficient  $C_p$  on the section surface is defined as :

$$C_p = \frac{P_s - P_0}{0.5\rho U^2} \quad (11)$$

where  $p_s$  is surface pressure,  $p_0$  is standard pressure at center point on inflow boundary.

The typical parts of section are defined as Area(a)-(c) in Fig. 10. Upper subdivision shows the mean value ( $\bar{C}_p$ ) and lower subdivision shows the fluctuating value as the standard deviation ( $C_p'$ ). The pressure distributions on (a) up and (b) down side sections are similar in Area(a)(b) just as the instantaneous vorticities shown in Fig. 8. In case of the tandem section, however, the surface pressure distributions both the mean and the fluctuation are very high around the leading corner of the down-wind side section in Area(c). Since the positive pressure acting on the front face of the down-wind side section in Area(c), the mean value of  $C_d$  on the tandem section is about two times as large as the single's one.

According as we point out that the phase difference between  $C_l$  and  $C_m$  is inversion in regard to both the single and tandem sections in Fig. 5, the harmonic fluid forces of  $C_l$  and  $C_m$  are generated by the fluctuating pressure on the surface that is located in the down-wind side to the center of the section. This fact is that a section body is drawn to a normal direction on a section surface where the sum total of negative pressure is the largest relatively. In case of the single box girder section, the

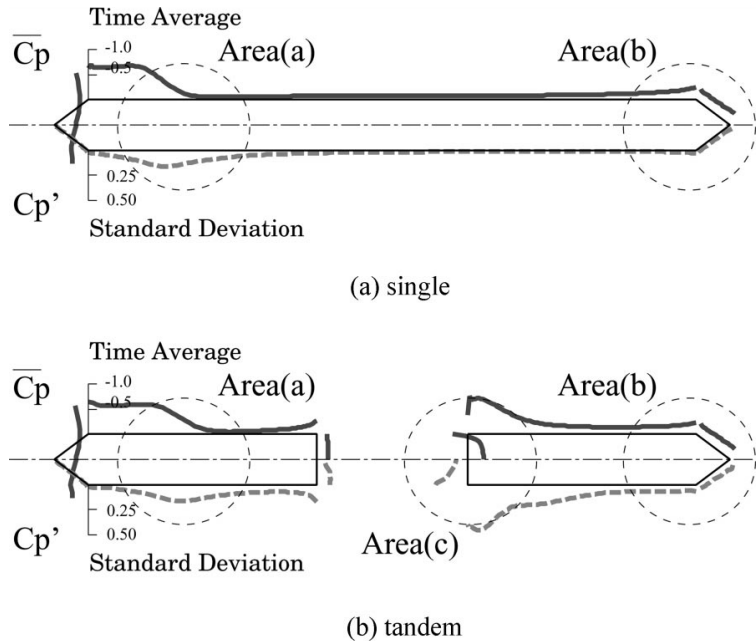


Fig. 10 Surface pressure distributions (upper: time average, lower: standard deviation)

standard deviation  $C_p'$  in Area(a) is the largest on the whole surface. But taking the phase difference between  $Cl$  and  $Cm$  into consideration, the fluctuating pressure of the trailing edge in Area(b) controls the harmonic fluid forces of  $Cl$  and  $Cm$ . The reason for this fact is that the constant separation-reattachment phenomenon in Area(a) do not interact between the upper and lower sides.

On the other hand, in case of the tandem section, it is cleared up that the harmonic fluid forces of  $Cl$  and  $Cm$  are caused by the interaction with the upper and lower surface pressure distributions in Area(c). It is considered that the alternate separating flows after the up-wind side section stream down and excite the harmonic separation-reattachment phenomenon in Area(c). And if the fluctuating pressure of the trailing edge in Area(b) controlled the harmonic fluid forces like the single section, the histories of  $Cl$  and  $Cm$  obtained by the both sections shown in Fig. 5 should be similar to each other.

## 5. Conclusions

In the present work three-dimensional numerical analysis of the flow around the single and tandem box girder sections are carried out to verify the generation mechanism of the fluctuating fluid forces. Finally, the following results are obtained.

- (1) The aerodynamics of the single and tandem box girder sections are quite different from each other. According to the presence of the central open space, the flow in the central open space is very complex in case of the tandem box girder section.
- (2) Since the positive pressure acting on the front face of the down-wind side section, the mean value of  $Cd$  on the tandem box girder section is about two times as large as the single's one. And the individual  $Cd$  on up and down wind side sections is almost equal.
- (3) The fluctuating amplitudes of  $Cl$  and  $Cm$  on the tandem box girder section are about 10 times the single's one, because of the large scale separation-reattachment phenomenon at the leading corner of the down-wind side section.
- (4) The separation from the front fairing and the reattachment to the each upper and lower surface around  $B/D=3$  are happened in common with the single and tandem box girder sections. Furthermore, the surface pressure distributions are also similar to each other as far as around the reattachment point to the rear of the leading edge.
- (5) In case of the single box girder section, the fluctuating pressure around the trailing edge controls the harmonic fluid forces of  $Cl$  and  $Cm$ . The reason for this fact is that the constant separation-reattachment flow from the front fairing do not interact between the upper and lower sides.
- (6) In case of the tandem box girder section, it is cleared up that the harmonic fluid forces of  $Cl$  and  $Cm$  are caused by the upper and lower surface pressure distributions around the leading corner of the down-wind side section. It is considered that the alternate separation flow after the up-wind side section excite the harmonic separation-reattachment phenomenon at the leading corner of the down-wind side section.

As the future work a forced oscillation analysis of a box girder section will be carried out by CFD, and generation mechanism of fluctuating aerodynamic forces accompanied by displacements will be discussed. Moreover the reason that tandem girders have a tendency to excels single girders in a wind-resistance stability will be also investigated.

This research is one of the works in the society for the study of "An Investigation on Wind-

Resistance and Economic Improvements of Super Long Span Bridges” that is composed of Public Works Research Institute, Honshu-Shikoku Bridge Authority, Public Works Research Center and eight private companies.

## References

- Diana, G., Falco, M., Cheli, F. and Cigada, A. (1999), “Experience gained in the Messina bridge aeroelastic project”, *Long-span Bridges and Aerodynamics*, 155-180.
- Hui, M.C.H. and Larsen, A. (2002), “Aerodynamic investigations for the deck of Stone-cutters bridge emphasizing Reynolds number effects”, *Proc. of the Second International Symposium on Advances in Wind and Structures*, 649-656.
- Ogawa, K., Shimodoi, H. and Oryu, T. (2002), “Aerodynamic characteristics of a 2-box girder section adaptable for a super-long span suspension bridge”, *J. Wind Eng. Ind. Aerodyn.*, **90**, 2033-2043.
- Sato, H., Hirahara, N., Fumoto, K., Hirano, S. and Kusuhara, S. (2002), “Full aeroelastic model test of a super long-span bridge with slotted box girder”, *J. Wind Eng. Ind. Aerodyn.*, **90**, 2023-2032.
- Matsumoto, M., Yoshizumi, F., Yabutani, K. and Nakajima, N. (1999), “Flutter stabilization and heaving-branch flutter”, *J. Wind Eng. Ind. Aerodyn.*, **83**, 289-299.
- Tamura, T., Itoh, Y. and Wada, A. (1995), “Three-dimensional simulation of an oscillating rectangular cylinder”, *Proceedings of the 6th International Conference on Flow-induced Vibration*.
- Hirano, H., Watanabe, S., Maruoka, A. and Ikenouchi, M. (1999), “Aerodynamic characteristics of rectangular cylinders”, *Int. J. CFD*, **12**, 151-163.
- Nakaguchi, H., Hashimoto, K. and Muto, S. (1968), “An experimental study on aerodynamic drag of rectangular cylinders”, *J. Japan Soc. Aeronaut Space Sci.*, **16**, 1-5(in Japanese).
- Bearman, P.W. and Trueman, D.M. (1972), “An investigation of the flow around rectangular cylinders”, *The Aeronautical Quarterly*, **23**, 229-237.
- Shirai, S. and Ueda, T. (2001), “Aerodynamic simulation by cfd on flat box girder of super-long span suspension bridge”, *Proc. of the 5th Asia-Pacific Conference on Wind Engineering*, 637-644.
- Xiang, H. and Ge, Y. (2002), “Refinements on aerodynamic stability analysis of super long-span bridges”, *J. Wind Eng. Ind. Aerodyn.*, **90**, 1493-1515.
- Maruoka, A., Hirano, H. and Watanabe, S. (1999), “Numerical fluid analysis for aerodynamic characteristics of a rectangular cylinder”, *Proc. of the 10th International Conference on Wind Engineering*, **2**, 1299-1306.
- Hayashi, M., Hatanaka, K. and Kawahara, M. (1991), “Lagrangian finite element method for free surface Navier-Stokes flow using fractional step methods”, *J. Num. Meth. Fluids*, **13**, 805-840.